scientific reports

OPEN

Novel accurate classification system developed using order transition pattern feature engineering technique with physiological signals

Mehmet Ali Gelen[1], Prabal Datta Barua[2], Irem Tasci[3], Gulay Tasci[4], Emrah Aydemir[5], Sengul Dogan[6]✉, Turker Tuncer[6] & U. R. Acharya[7]

This paper presents a novel, explainable feature engineering framework for classifying EEG and ECG signals with high accuracy. The proposed method employs the Order Transition Pattern (OTPat) feature extractor. The presented OTPat feature extractor captures both channel/column-based patterns (spatial features) using all channels for each point and signal/row-based patterns (temporal features) by extracting features from individual channels using overlapping blocks. The extracted features are then refined using cumulative weighted iterative neighborhood component analysis (CWINCA) for feature selection and classified with a t-algorithm k-nearest neighbors (tkNN) classifier. Finally, two symbolic languages, Directed Lobish (DLob) and Cardioish, generate interpretable results in the form of cortical and cardiac connectome diagrams. The OTPat-based XFE model achieves over 95% accuracy on several EEG and ECG datasets and reaches 86.07% accuracy on an 8-class EEG artifact dataset. These results demonstrate high performance and clear interpretability, highlighting the model's potential for robust biomedical signal classification.

Keywords OTPat, Explainable feature engineering, Biomedical signal classification, TkNN, Directed lobish, Cardioish

Biomedical signals such as EEG (electroencephalography) and ECG (electrocardiography) are crucial for understanding brain and heart functions, respectively[1,2]. These signals are widely used in medical diagnosis to detect various conditions, such as neurological disorders and heart diseases[3]. Despite their importance, it is difficult to analyze them accurately due to their complex structure and inter-individual variability[4].

Recently, researchers have focused on developing advanced techniques to process and classify biomedical signals[5–8]. These efforts aim to increase the sensitivity of the analysis while ensuring that the results are interpretable and clinically meaningful[3]. Achieving high accuracy and interpretability of the developed system is important in healthcare[9].

There is a growing need for methods that can process data from multiple sources, such as EEG and ECG, in a unified manner[10]. This can help to provide a more accurate diagnosis of complex medical conditions[11]. Hence, there is a need for an efficient and explainable approach[12].

Although most of the presented automatic biomedical signal classification research reported high accuracies under controlled conditions, they have several limitations[13]. They require high computational power since most use deep learning models to achieve high classification performances. They lack subject-specific validation, offer limited interpretability and rely on a single modality. A detailed look at these issues shows that multimodal approaches are needed. Such approaches can improve generalizability and interpretability with lower computational complexity.

[1]Department of Cardiology, Elazig Fethi Sekin City Hospital, Elazig, Turkey. [2]School of Business (Information System), University of Southern Queensland, Toowoomba, Australia. [3]Department of Neurology, School of Medicine, Firat University, Elazig, Turkey. [4]Department of Psychiatry, Elazig Fethi Sekin City Hospital, Elazig, Turkey. [5]Department of Management Information Systems, Management Faculty, Sakarya University, Sakarya, Turkey. [6]Department of Digital Forensics Engineering, Technology Faculty, Firat University, Elazig, Turkey. [7]School of Mathematics, Physics and Computing, University of Southern Queensland, Springfield, Australia. ✉email: sdogan@firat.edu.tr

In this work, our primary goal is to develop a general explainable feature engineering (XFE) model for biomedical signals. For this purpose, ECG and EEG signal datasets, which are frequently used in the literature, were utilized. A new method, Order Transition Pattern (OTPat), is proposed to automatically classify these signals. This method is designed to identify meaningful transitions between signal channels and within signals, focusing on meaningful feature extraction.

To achieve high classification performance, cumulative weighted iterative neighborhood component analysis (CWINCA)[14] is used as a self-organized feature selector, along with t-algorithm k-nearest neighbors (tkNN)[15] as a self-organized classifier. Since EEG and ECG datasets are employed as test datasets in this study, explainable results are derived using the Directed Lobish (DLob)[16] and Cardioish[17] symbolic languages. Both symbolic languages are purpose-oriented explainable artificial intelligence (XAI) methods that create connectome diagrams based on the selected features.

Related works

There are various studies conducted across different disciplines[18–21], focusing on diverse applications ranging from healthcare to cognitive sciences and neurotechnology[22–24]. Brain-Computer Interface (BCI) systems[25–27] has gained significant attention due to its ability to decode neural activity and facilitate interaction between the brain and external devices[28–31]. Various machine learning-based approaches have been proposed for stress detection[32], mental performance assessment[33], and neurodegenerative disease classification[34–36], including amyotrophic lateral sclerosis (ALS). These studies leverage electrophysiological signals, such as electroencephalography (EEG)[37–39] and electromyography (EMG)[40], to extract meaningful patterns associated with cognitive and motor impairments.

We have presented a few machine learning-based studies related to the detection of stress, mental performance and ALS in this section.

Mane and Shinde[41] introduced a hybrid convolutional neural network (CNN)- long short-term memory (LSTM)-based model for EEG-based stress detection. They used SEED and DEAP datasets to detect stress levels, and their model yielded 97.8% classification accuracy with 10-fold cross-validation (CV) strategy. They did not employ the subject- or record-wise validation techniques and also did not employ explainable artificial intelligence (XAI) methods.

Badr et al.[42] reviewed deep learning techniques, particularly CNN and LSTM models, for mental stress detection using EEG signals. They analyzed studies employing various data representations and showed that spectral and topographical inputs can obtain up to 88% accuracy. Their findings emphasized the potential of using advanced EEG input representations and hybrid models for stress detection with high accuracy and generalizability. However, they only focused on EEG signals. Moreover, they didn't use any XAI methods to present interpretable results.

Malviya and Mal[43] presented a CNN– Bidirectional LSTM hybrid model for stress detection using EEG signals with the Physionet dataset. Their model used discrete wavelet transform (DWT) for denoising and feature extraction, followed by CNN for feature selection and BLSTM for classification. Their approach achieved a high accuracy of 99.20%. They used only EEG signals and did not employ XAI results nor subject-wise validations.

Roy et al.[44] proposed a hybrid deep learning approach combining CNN, LSTM, BiLSTM, and gated recurrent unit (GRU) layers for stress detection using the STEW EEG dataset. Their model used DWT for feature extraction and achieved an accuracy of 98.10%. However, they used only one EEG dataset.

Fernandez et al.[45] investigated students' stress detection using EEG signals recorded during stress-inducing activities with machine learning models. They used features such as mean and standard deviation from EEG channels and achieved an accuracy of 86.24% using the light gradient-boosting machine. XAI results or subject-wise validations were not performed. Furthermore, the models were evaluated solely on EEG signals and combined three deep learning architectures, which increased the overall time complexity.

Patel et al.[46] proposed a hybrid deep learning approach by combining 1D CNN with BiLSTM and BiGRU for mental stress detection using the DEAP dataset. They utilized sliding FFT (fast Fourier transform) for feature extraction across 14 EEG channels and classified stress states into four categories. The 1D CNN + BiLSTM model achieved the highest accuracy of 88.03%. However, they only focused on EEG signals.

Al-Saggaf et al.[47] evaluated EEG-based stress detection approaches for wearable devices using a dataset recorded during stress-inducing tasks. Their method achieved the highest accuracy of 96% using the machine learning method and completed the process fast (0.32 s). They used only the EEG dataset and did not employ XAI methods.

Opałka et al.[48] developed a multi-channel CNN architecture for EEG-based mental task classification using the BCI Competition III Dataset V. Their model focused on frequency-domain sub-band analysis and employed a two-layer CNN structure to improve feature extraction. Their approach achieved a classification accuracy of nearly 70%. Their study showed lower classification accuracy, with no interpretable results.

Zhang et al.[49] proposed a hybrid deep learning model, Recurrent 3D CNN, combining recurrent and 3D convolutional neural networks for cross-task mental workload assessment using EEG data from n-back and arithmetic tasks. Their method transformed EEG signals into spatial-spectral-temporal features and achieved an average classification accuracy of 88.9%. Their study focused on limited tasks (spatial n-back and arithmetic) with higher time complexity.

He et al.[50] developed a CNN-based method for real-time acute cognitive stress detection using ECG signals. The study utilized a super-short 10-second window of ECG data from 20 participants under stress-inducing arithmetic tasks. Their proposed CNN model achieved a 17.3% error rate, outperforming conventional heart rate variability-based methods by at least 7.2%. The limitation of their study is the high computational load of the CNN model and their model has no multimodal biomedical signal classification option.

Bergil et al.[51] analyzed the performance of arithmetic and mental tasks using EEG and ECG signals from the PhysioNet database, including 36 participants. They extracted wavelet-based features and achieved a classification accuracy of 99% using a k-NN classifier using EEG and ECG features. The limitation of their study is the reliance on high-dimensional feature sets derived from wavelet transforms of EEG and ECG signals. They used both EEG and ECG signals, but they have no subject-wise and interpretable results.

Pirasteh et al.[52] reviewed EEG-based brain-computer interface (BCI) methods developed for the rehabilitation of advanced ALS patients by enabling communication and environmental control. They discussed various feature extraction techniques, including common spatial patterns and wavelet packet decomposition, and classifiers like support vector machine (SVM) and neural networks, highlighting SVM's robustness with high-dimensional data. Although accuracy rates varied across different approaches. Hybrid methods that combine EEG modalities showed potential for improved performance. Their study highlighted the benefits of BCIs for ALS patients. This is true despite challenges such as signal instability and device usability. Also, their review didn't focus on XAI and subject-wise validation.

Literature gaps

Based on our literature review, we have identified the below gaps:

- Nowadays, deep learning techniques have been widely used in biomedical signal classification[53,54], as deep learning models have achieved high classification performance[55]. However, these models have a high time burden[56].
- Most of the works focused on either EEG or ECG signal classification[57–59]. Hence, multimodal signal classification is needed.
- In most signal classification models, researchers are motivated to achieve high classification performance[60,61]. There are limited explainable models. Most of the explainable models have used well-known explanation generation methods such as Grad-CAM (Gradient-weighted Class Activation Mapping), Lime (Local Interpretable Model-agnostic Explanations), and SHAP (Shapley Additive Explanation)[62–64]. The number of specialized (data-driven) explainable methods is limited.

Motivation and study outline

We have proposed a novel feature extraction function, OTPat, to address the literature gap. OTPat aims to extract meaningful features from both channels and signals using an ordering approach. The extraction of features from both channels and signals yields informative features. To demonstrate the classification ability of the presented OTPat, an XFE model has been developed. In this model, features were extracted using OTPat, and the most informative features were selected by the CWINCA[14] feature selector and classification was performed using tkNN[15]. We introduced a highly accurate feature engineering model by combining these three stages.

We were inspired by self-organized machine learning models to propose this signal classification model. We integrated the self-organized feature selector (CWINCA) and classifier (tkNN) with the proposed OTPat. Due to this self-organized nature, we have developed a highly accurate model that can compete with the classification performance of deep learning models. Moreover, the presented OTPat-driven XFE model has linear time complexity.

To address the second gap, we used both EEG and ECG datasets to demonstrate the general classification ability of the introduced OTPat-driven XFE model.

To address the last gap, we used DLob[16] and Cardioish[17] XAI methods to obtain interpretable results. DLob is an EEG-related XAI method, while Cardioish is a symbolic language-based explainable results generator for ECG signals. By employing DLob and Cardioish, we bridged the third literature gap and obtained highly insightful XAI results. To generate interpretable results, we integrated the DLob/Cardioish symbolic languages into the recommended biomedical signal classification model. In this work, connectome diagrams were generated using the DLob/Cardioish symbol sequences. Additionally, the information entropy of these DLob/Cardioish strings was calculated, showcasing the complexity of psychosis-related criminal detection.

The presented OTPat-driven XFE model consists of four phases: (i) feature extraction based on OTPat, (ii) selection of the most informative features using the CWINCA feature selector, (iii) tkNN-based classification outcome generation, and (iv) interpretable results generation using DLob/Cardioish.

By deploying OTPat alone, we extracted features from channels and signals. To select the most informative features, the CWINCA feature selector was applied. This feature selector is self-organized as it automatically identifies the best-selected feature vector instead of preselected feature vectors. These selected features were used for both classification and XAI result generation. In the classification phase, tkNN was utilized to generate classification results. This classifier is both ensemble and iterative, generating multiple classification outputs and automatically selecting the most accurate outcome. In this respect, tkNN is a self-organized classifier. By employing self-organized feature selection and classification, we enhanced the classification ability of the introduced OTPat-based XFE framework.

Therefore, this model is highly accurate and serves as a competitive feature engineering alternative to deep learning models. In the final phase, the identities of the selected features were used to create DLob or Cardioish symbol sequences. Subsequently, connectome diagrams and information entropies were generated for the datasets used.

Innovation and contributions

Innovation

- Proposed a new generation OTPat feature extraction function which used advanced ordering-based transformations to capture subtle channel-level (spatial) or single-channel (temporal) patterns. This approach combined local and global signal characteristics with minimal computational overhead.
- Introduced a novel OTPat-based XFE pipeline for EEG and ECG classification. This pipeline is self-organized via CWINCA for feature selection and tkNN for classification. It yielded state-of-the-art accuracy across multiple datasets while maintaining linear time complexity.
- Used DLob and Cardioish symbolic languages in a single framework. This is the first approach to produce detailed connectome diagrams for both EEG and ECG signals. It equips clinicians and researchers with clearer, more interpretable insights into underlying physiological processes.

Contributions

- The introduced OTPat-based XFE framework is scalable, as it has been tested on various EEG and ECG signal datasets. Moreover, the recommended model achieved over 95% classification accuracy on the biomedical signal datasets. Hence, the presented model contributes to the biomedical signal classification field, offering an alternative to deep learning models.
- The integration of DLob and Cardioish provides medical insights from the datasets, which are XAI-driven findings. Hence, the proposed OTPat-driven XFE model contributes to medicine by generating explainable results based on feature engineering.

The used datasets

To develop the proposed OTPat-driven XFE model, we used two EEG and one ECG dataset. The details of these datasets are provided below. These datasets were used to demonstrate the general biomedical signal classification ability of the recommended OTPat-driven XFE framework.

EEG stress dataset

In this study, the EEG stress dataset was used[65,66]. This dataset consisted of 310 participants (150 stressed and 160 controls) who were survivors (disaster victims) of the February 6 earthquake series in Turkey. The EEG signals were divided into 15-second segments. In this study, we used 3,667 EEG segments (1,785 stress and 1,882 control), with participants' ages ranging from 18 to 43 years.

EEG ALS dataset

The Amyotrophic Lateral Sclerosis (ALS) EEG detection dataset has two classes: (i) ALS and (ii) control[67,68]. This dataset is unbalanced, including 170 healthy participants and 6 ALS participants. The EEG signals were segmented into 10-second intervals. Consequently, 10,248 EEG segments were obtained from the healthy group and 2,631 EEG segments from the ALS group. To balance the EEG ALS dataset, we randomly selected 2,631 EEG segments from the healthy group. As a result, we created a balanced EEG ALS dataset containing 5,262 EEG segments. This dataset was collected using a brain cap with 32 channels inthe Emotiv Flex 32-channel brain cap.

ECG mental health dataset

The ECG mental health classification dataset consists of four classes: normal, bipolar, depression, and schizophrenia[69]. The dataset consists of 2926 ECG beats with 900 (normal), 197 (bipolar), 202 (depression), and 1,607(schizophrenia) ECG beats collected using 12 channels. The ECG beats were collected from 198 participants with mental health disorders (119 with schizophrenia, 62 with bipolar disorder, and 17 with depression) aged between 18 and 80 years.

Proposed OTPat feature extractor

The primary objective of this feature extractor is to generate hidden patterns to get high classification performance. The main innovation of this work is the OTPat. This feature extractor extracts features from both single and multi-channel signals. The introduced OTPat captures relationships from signal values and channels. The general steps of the presented model are (i) spatial feature extraction, (ii) temporal feature extraction, and (iii) feature concatenation. Figure 1 presents the graphical representation of the OTPat feature extractor.

Figure 1 presents the graphical depiction of the recommended OTPat, and the steps of this feature extractor are outlined below.

Step 1: Define the transition table since the utilized OTPat is a transition table feature extraction-based method.

$$tt_q = \begin{bmatrix} 0 & \cdots & 0 \\ \vdots & \ddots & \vdots \\ 0 & \cdots & 0 \end{bmatrix}, q \in \left\{1,2,\ldots,\mathtt{C}+1\right\} \tag{1}$$

where tt: transition table and $\mathtt{C}$: the number of channels. Herein, each transition table has been defined as a counter.

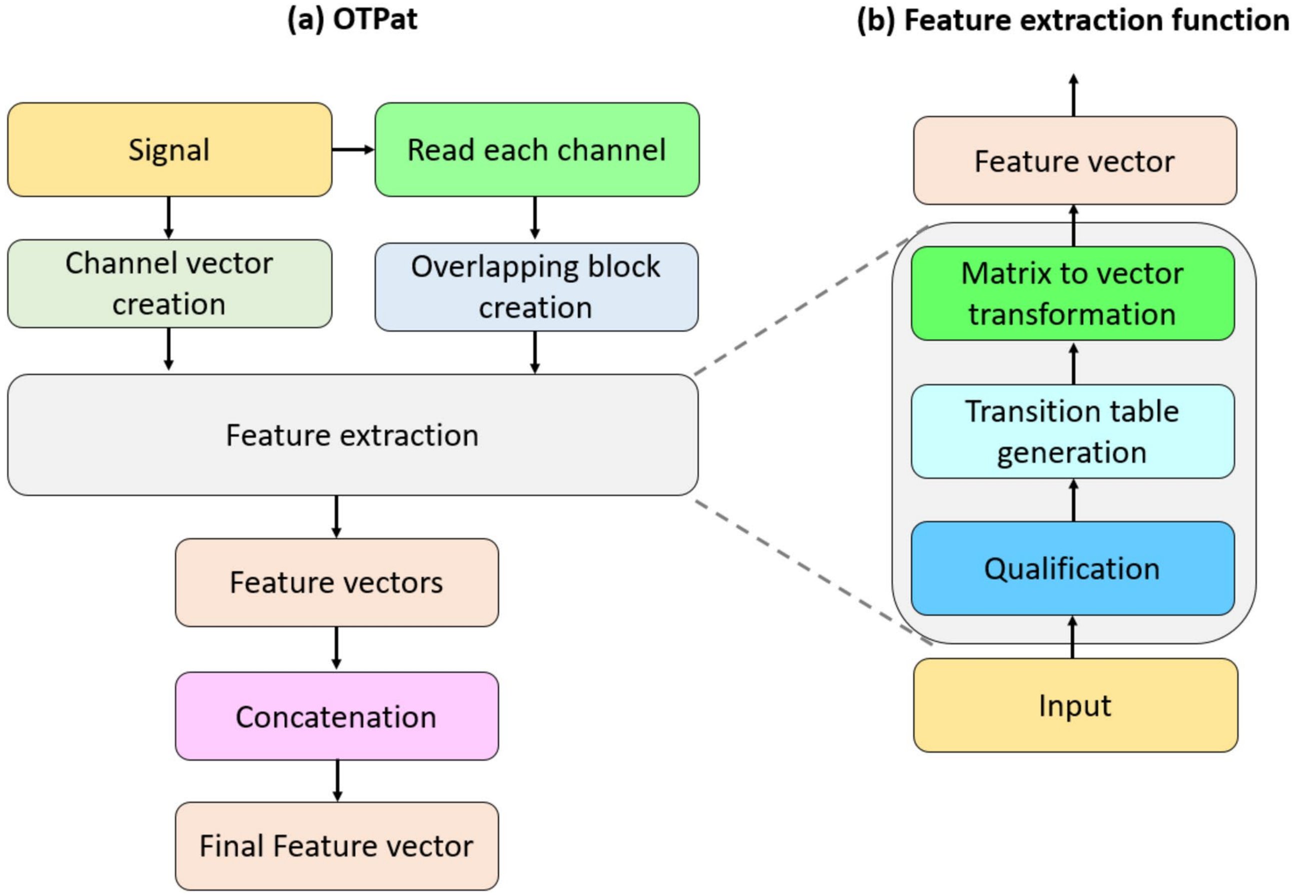

Fig. 1. Graphical representation of proposed OTPat feature extractor.

Step 2: Create a channel/column vector to extract spatial features. In the feature extraction process, ordering transformer and transition table feature extraction have been utilized together. In this step, channel vector creation has been defined as below. The column-based feature extraction has been defined in Step 3.

$$cv^i = signal\,(i,:)\,,\ i \in \{1,2,\ldots,len\} \tag{2}$$

Herein, cv: channel vector, len: length of the signal.

Step 3: Generate spatial features using the ordering transformer, transition table extraction, and matrix-to-vector transformation.

In this step, a channel vector from each time point is passed through the ordering transformer. The resulting transitions are recorded in a transition table, which is then flattened into a feature vector. This process encapsulates the inter-channel (column-based) relationships and prepares the data for subsequent feature selection and classification.

$$id = argmax\left(-cv^i\right) \tag{3}$$

$$tt_1\left(id\left(h\right),id\left(h+1\right)\right) = tt_1\left(id\left(h\right),id\left(h+1\right)\right)+1, h \in \{1,2,\ldots,len-1\} \tag{4}$$

$$fvec^1\left(z\right) = tt_1\left(a,b\right),\ z \in \left\{1,2,\ldots,\mathbb{C}^2\right\}, a \in \left\{1,2,\ldots,\mathbb{C}\right\}, b \in \left\{1,2,\ldots,\mathbb{C}\right\} \tag{5}$$

where id: the qualified indices, and $fvec$: feature vector with a length of. In the spatial (channel-based) feature extraction, the first feature vector ($fvec^1$) has been created. The temporal (row-based) feature extraction mode of the presented OTPat has been explained in Step 4 and Step 5.

Step 4: Read each channel and create overlapping block with a length of number of channels. The generated overlapping blocks have been utilized as input of the ordering transformer.

$$bl_c^i = signal\left(i+j-1,c\right),\ j \in \left\{1,2,\ldots,\mathbb{C}\right\},\ c \in \left\{1,2,\ldots,\mathbb{C}\right\} \tag{6}$$

Herein, bl: overlapping block with a length of $\mathbb{C}$.

Step 5: Extract features deploying ordering feature generation approximation.

$$id = argmax\left(-bl_c^i\right) \tag{7}$$

$$tt_{c+1}\left(id\left(h\right), id\left(h+1\right)\right) = tt_{c+1}\left(id\left(h\right), id\left(h+1\right)\right) + 1, \tag{8}$$

$$fvec^{c+1}\left(z\right) = tt_{c+1}\left(a, b\right) \tag{9}$$

In the row-based feature extraction mode, $\mathtt{C}$ feature vectors have been created. To obtain the final feature vector, these generated features have been merged and this process is defined in Step 6.

Step 6: Concatenate the extracted feature vectors and create the final feature vector.

$$feat\left(q + \mathtt{C}\ \left(z-1\right)\right) = fvec^q\left(z\right) \tag{10}$$

where $feat$: the extracted final feature vector.

The OTPat feature extractor produces a final feature vector with a dimensionality of $\mathtt{C}^{\,3} + \mathtt{C}^{\,2}$, extracting both spatial (channel-based) and temporal (signal-based) patterns from the physiological signals.

The presented OTPat is a transition table–based feature extraction method that extracts both spatial and temporal patterns from physiological signals. Initially, a transition table is defined as a counter matrix to record changes in the ordering of channel values. In the channel-based (spatial) mode, a channel vector is generated at each time point and processed using an ordering transformer; the resulting ordered indices update the transition table, which is then flattened into a feature vector representing inter-channel relationships.

In the signal-based (temporal) mode, overlapping blocks are created from each channel's time-series data. Each block is processed similarly, using the ordering transformer to update a separate transition table converted into additional feature vectors. Finally, the channel-based and signal-based feature vectors are concatenated to form a final feature vector with the dimensionality of $\mathtt{C}^{\,3} + \mathtt{C}^{\,2}$. This OTPat feature extraction method generates the spatial distribution across channels. It also captures the temporal dynamics within each channel. This dual extraction increases the model's robustness for biomedical signal classification.

OTPat-based explainable feature engineering model

A new OTPat-based explainable feature engineering (XFE) model has been introduced to evaluate the classification capability of the proposed OTPat. The introduced OTPat-based XFE framework comprises four main phases:

- Feature extraction using the recommended OTPat,
- CWINCA-based feature selection,
- Classification using tkNN,
- Explainable artificial intelligence (XAI) results generation using symbolic languages (DLob and Cardioish).

Figure 2 shows the schematic diagram of the introduced OTPat-based XFE framework.

Figure 2 illustrates that the features are generated using the OTPat feature extraction method. This method extracts both spatial (channel-based) and temporal (signal-based) features. To improve the classification ability of the OTPat-centric XFE model, we have used CWINCA for feature selection and tkNN for classification. The reasons for selecting these methods are as follows: - NCA and kNN are distance-based. They measure the distances between data points, which help to achieve high classification performance when used together. CWINCA and tkNN are advanced versions of NCA[70] and kNN[71]. They are self-organized and iterative models. CWINCA chooses the most important features using cumulative weights. tkNN classifies the selected features through iterative majority voting. These improvements make the models more robust and effective. To enhance classification abilities, we have combined OTPat, CWINCA, and tkNN. To generate interpretable results, we used symbolic language-based XAI generation methods. In this work, we used DLob and Cardioish symbolic languages for XAI, and the resulting interpretable information related to the brain and heart was computed.

Figure 2 shows that features are generated by the OTPat feature extraction method. This method extracts both spatial features (channel-based) and temporal features (signal-based). We used CWINCA as the feature selector and tkNN as the classifier to improve accuracy.

NCA and kNN are distance-based methods. They work by measuring distances between data points. This helps them achieve high classification performance when used together.

CWINCA and tkNN are advanced versions of NCA and kNN. They are self-organized and iterative. CWINCA selects the most important features using cumulative weights. tkNN classifies the selected features using iterative majority voting. These improvements make the models more robust and effective.

We combined OTPat, CWINCA, and tkNN to improve the classification performance.

For interpretability, we use a symbolic language-based XAI method. In this study, we used DLob and Cardioish as XAI methods. The interpretable results for the brain and heart are computed using these symbolic languages.

The details of these phases are given below.

Phase 1: Extract features from each signal using the OTPat feature extractor.

$$X\left(d,:\right) = OTPat\left(signal\right),\ d \in \ \{1,2,\dots\ ,Dim\} \tag{11}$$

where, $OTPat(.)$: OTPat feature extraction function, Dim : number of biomedical signals and X: feature matrix.

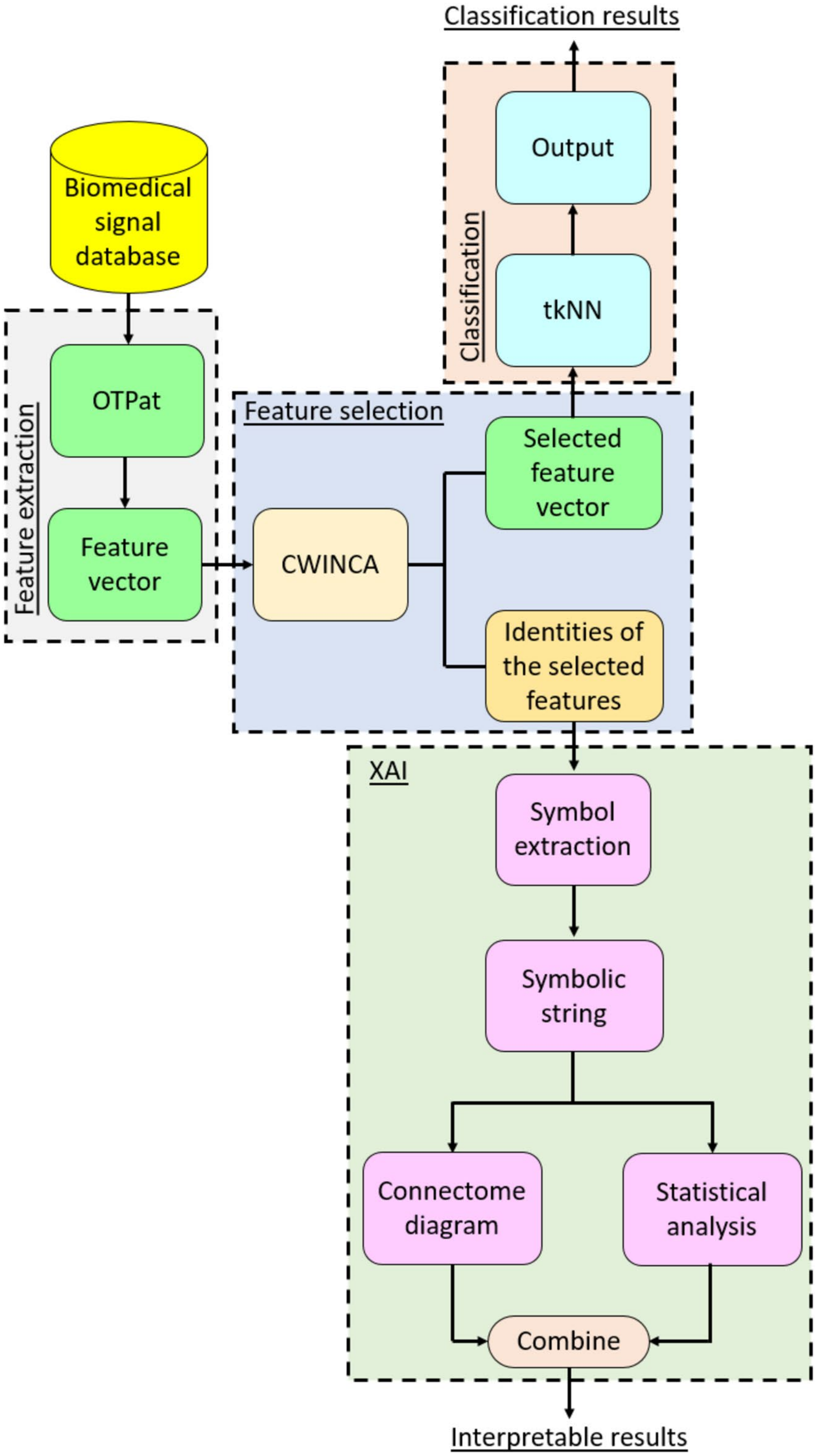

Fig. 2. Overview of the introduced OTPat-based XFE framework.

Phase 2: Choose the most informative features deploying the CWINCA feature selector. CWINCA is a self-organized feature selection method that combines the flexibility of an iterative approach with the importance weights of features[14,16]. First, it normalizes the extracted features using min–max scaling/normalization. Then, NCA is applied to assign a weight to each feature, reflecting its relevance to the classification task. These weights are then sorted to produce an ordered list of features. CWINCA uses cumulative weight thresholds (0.75 and 0.99) to determine a range of possible feature subset sizes. Within that range, each subset is tested using a kNN classifier, and its classification accuracy is computed. CWINCA automatically selects the subset that achieves the highest accuracy, finalizing the best feature vector for subsequent classification and explainable result generation.

$$sX = \psi\left(X, y\right) \tag{12}$$

Herein, sX: selected feature matrix, $\psi\left(.\right)$: CWINCA feature selection function and y: actual/real outputs. The working of the CWINCA feature selector is given below.

Input: The extracted features (X).

Output: The selected feature vector (sX).

$X^N = \frac{X(:,i) - min\left(X(:,i)\right)}{max\left(X(:,i)\right) - min\left(X(:,i)\right) + \varepsilon}$

// Normalize the extracted features by deploying min-max normalization. Herein, X^N: Normalized feature matrix

$w = NCA(X^N, y);$

// Generate weights (w) deploying NCA ($NCA(.)$) feature selector.

$x = argmaxg(-weight);$

// Apply ordering and obtain the qualified indices (x) of the feature weights.

$start = CumW(X^N, w, x, 0.75);$

$stop = CumW(X^N, w, x, 0.99);$

// Herein, $CumW(.)$: cumulative weight-based number of feature detection functions $start$: start value of the loop and $stop$: stop value of the loop. The threshold values used to compute these start and stop values are 0.75 and 0.99, respectively.

for i= $start$ to $stop$ **do**

    for j= 1 to i **do**

        $sf^{i-start+1}(:, j) = X^N\left(:, x(j)\right);$

// Select the features iteratively and sf is a selected feature vector.

    end for j

    $cac(i) = kNN\left(sf^{i-start+1}\right);$

// Compute the classification accuracies (cac) of the selected feature vectors deploying kNN ($kNN(.)$) classifier.

end for i

$id = argmax(cac);$

// Compute the index (id) of the classification accuracies.

$sX = sf^{id};$

Algorithm 1. CWINCA feature selection procedure[14,16].

CWINCA begins by applying a min-max normalization to each feature in the dataset. It then uses a neighborhood component analysis method to assign a weight to each feature. The next step sorts the features based on these weights from highest to lowest. After sorting, the method determines two threshold points at 0.75 and 0.99 for the cumulative weight. It marks the lower threshold as the start value and the upper threshold as the stop value. It then loops through different feature subset sizes in the range between the start and stop values. For each subset size, it selects the most important features and evaluates them using a kNN classifier. It records the classification accuracy for every tested subset. Finally, it picks the feature subset with the highest accuracy and designates it as the final selected set of features.

Algorithm 1 demonstrates that the employed CWINCA feature selector is a self-organized feature selection function. It generates multiple selected features and automatically identifies the best features from the chosen ones. The feature selection phase feeds into the classification (Phase 3) and XAI (Phase 4) phases.

Phase 3: Classify the selected features by using the self-organized tkNN classifier.

$$out = \ell(sX, y) \tag{13}$$

where, out: the generated classification outcome and $\ell(.)$: tkNN classifier.

The procedure of the tkNN classifier has been demonstrated in Algorithm 2.

Input: The selected features (sX).

Output: Classification outcome (out).

$t = 1$;
// Counter definition
for each a in $D = \{City\ Block, Eudlidean, Cosine\}$ **do**
// Defining distances. In this work, we have used the above distances.
  for each b in $W = \{Inverse, Squared\ Inverse, Equal\}$ **do**
// Definition of the weights. In this work, we have used the above weights.
    for each c in $k = \{1,2, \dots ,10\}$ **do**
// Definition of the weights. In this work, the utilized k values from 1 to 10.
      $paro_t = kNN(sX, D_a, W_b, k_c)$;
// Creation parameter-based outcomes ($paro$) by changing the parameters.
      $t = t + 1$;
    end for c
  end for b
end for a
$cac = \gamma(paro, y)$;
$dx = argsort(-cac)$
// Herein, classification accuracy computation has been defined and $\gamma(.)$: classification accuracy computation function and the qualified indices of parameter-based outcomes according to the classification accuracy.
for i=3 to $t - 1$ **do** // Applying iterative majority voting
  $array = [paro_{dx(1)}, paro_{dx(2)}, \dots , paro_{dx(i)}]$;
// Creating an array for majority voting.
  $vo_{i-2} = \varpi(array)$;
// Herein, vo: voted outcome and $\varpi(.)$: mode function.
  $cac(t + i - 2) = \gamma(vo_{i-2}, y)$;
// Classification accuracy computation.
end for i
$qx = argmax(cac)$;
// Computation index (qx) of the maximum classification accuracy.
if $qx < t$ **then**
  $out = paro_{qx}$;
else
  $out = vo_{qx-t-1}$;
end if

Algorithm 2. The procedure of the tkNN classifier[15].

Algorithm 2 showcases that the used tkNN is a self-organized classifier.

Phase 4: Generate explainable results by deploying the identities of the selected features. The index to symbol conversion has been given below.

$$id_1^k = [x(k) - 1] \left(mod\ \complement \right) + 1,\ k \in \{1,2, \dots , nos\} \tag{14}$$

$$id_2^k = \left\lfloor \frac{x(k)-1}{\mathtt{C}} \right\rfloor \left(mod\, \mathtt{C} \right) + 1 \tag{15}$$

Herein, id: index of the look-up-table and nos: number of selected features. By utilizing these computed indexes, DLob or Cardioish symbol sequences have been generated as below.

$$Seq\,(1 + 2\,(k-1)) = LUT\left(id_1^k\right) \tag{16}$$

$$Seq\,(2k) = LUT\left(id_1^k\right) \tag{17}$$

Herein, Seq: the created symbolic language string, LUT: look-up-table.

The histogram of these symbols and the information entropy of the created string were then computed. Additionally, connectome diagrams were produced by calculating the transition table of the generated symbolic language string.

In this work, we used DLob and Cardioish, and the meanings of the symbols in these symbolic languages are provided in Table 1.

Table 1 presents 16 and 12 symbols in the DLob and Cardioish symbolic languages, respectively. The number of symbols can be reduced depending on the specific ECG device or brain cap.

The four phases defined above constitute the recommended OTPat-driven model.

Experimental results

The explainable and classification results obtained using our developed OTPat-driven XFE model on the EEG and ECG datasets are presented in this section.

We implemented the presented OTPat-driven XFE model in the MATLAB (version 2024a) programming environment on a computer with a 2.8 GHz CPU and 32 GB of RAM running Windows 11. The parameters used in this model are as follows:

Symbols	Meaning
DLob	FL: Decision making, planning and logical reasoning.
	FR: Problem-solving, emotional regulation and creative thinking.
	Fz: Cognitive control and focus.
	TL: Language comprehension and auditory memory.
	TR: Social cues, non-verbal memory and emotional memory.
	PL: Language interpretation, spatial reasoning and sensory processing.
	PR: Attention and sensory integration (touch and body awareness).
	Pz: Sensory integration and central processing of spatial awareness.
	OL: Color, pattern and shapes visual processing.
	OR: Visual recognition and spatial processing.
	Oz: Primary visual integration and focus.
	CL: Transition of sensory to cognitive processes in the left hemisphere.
	CR: Transition of sensory to cognitive processes in the right hemisphere.
	Cz: Interhemispheric integration.
	AL: Auditory processing behind the left ear.
	AR: Auditory processing behind the right ear.
Cardioish	Ld1 (Lead I): Monitors the effects of sympathetic activation on the heart. It represents the left atrium and left ventricle.
	Ld2 (Lead II): Overall heart rhythm and P-wave activity.
	Ld3 (Lead III): It defines the inferior wall of the hearth.
	AVR: The base of the heart and right ventricle.
	AVL: Left ventricle and upper lateral wall.
	AVF: Left ventricle and inferior wall.
	V1S (Lead V1): Septum and right ventricle activation.
	V2S (Lead V2): Anterior septal region activation.
	V3A (Lead V3): Anterior wall.
	V4A (Lead V4): Left ventricle and the mitral valve region.
	V5L (Lead V5): It is used in lateral ischemia or hypertrophy analysis.
	V6L (Lead V6): It analyzes the impact of chronic conditions (e.g., diabetes, hypertension) on the left ventricle.

Table 1. Meaning of the DLob and cardioish symbols[17].

OTPat

In this feature extraction function, there are two feature extraction modes: spatial (column-based, using all channels to extract features) and temporal (using individual channel signals). In the channel/column-based mode, an ordering transformer is applied to the channel vector of each point, resulting in a transformed signal. In the row-based mode, overlapping blocks are created, and an ordering transformation is applied to each block to generate transformed signals. In the transformer phase, +1 transformed signals are created. To generate features from each transformed signal, a transition table feature extractor is used which produces $\mathbb{C}^3 + \mathbb{C}^2$ features for each EEG signal.

CWINCA

CWINCA is a self-organized, iterative feature selection function[14]. The range of the loop for iterative feature selection is determined by a cumulative weight computation, using threshold values of 0.75 and 0.99 to identify start and stop points. In this iterative selection, a kNN classifier with 10-fold cross-validation is used to compute classification accuracy for each subset of features. The best feature subset is chosen based on these accuracies obtained.

tkNN

This classifier generates parametric and voted outcomes[15]. To produce parametric outcomes, a parameter iteration is run with 3 distances, 3 weights, and 10 k-values, yielding 90 parameter-based outcomes. Using iterative majority voting (IMV), 88 voted outcomes are generated, totaling 178 (=90+88) outcomes. The classification accuracy of each is computed, and the outcome with the highest accuracy is selected using a greedy algorithm.

XAI method

This method applies channel-to-DLob/Cardioish symbol transformation because OTPat-generated features include channel/lead information[16,17]. The identities of the selected features are extracted and used to construct the DLob/Cardioish symbols. The histogram and transition table of these symbols are then created, and information entropy is computed using the histogram. The transition table forms a connectome diagram, in which each DLob/Cardioish symbol represents a specific cortical or cardiac region, thereby offering interpretable insights. This research, 14 DLob symbols were used for the EEG ALS dataset, 8 for the other EEG datasets, and 12 Cardioish symbols for the ECG dataset (matching the 12 ECG leads).

The following parameters affect the classification performance of the recommended OTPat-centric XFE framework:

- OTPat: The choice between spatial (column-based) and temporal (row-based) extraction influences the type of features generated. For the temporal approach, the size and overlap of blocks can impact the performance.
- CWINCA: Threshold points and the classifier's parameters can affect classification performance.
- tkNN: In the utilized kNN, 90 parametric outcomes have been generated. Increasing the number of parameters can lead to higher classification performance. Additionally, parameter tuning can be applied to the tkNN classifier.

First, we analyzed the computational complexity of the model in different phases.

In the **feature extraction phase**, OTPat is applied to each signal. This results in a complexity of $O(D \cdot L \cdot C)$. Here, D is the number of signals, L represents the length of each signal and C is the number of channels.

In the **feature selection phase**, the CWINCA selector works with a complexity of $O(N \cdot D + R \cdot K \cdot D + L \cdot D)$. In this case, N represents the complexity of the NCA algorithm, R is the number of iterations and K is the complexity of the kNN classifier.

In the **classification phase**, the tkNN classifier generates parameter-based outcomes. It also performs iterative majority voting (IMV), which has a complexity of $O(P \cdot K + I)$. Here, P is the number of parameters and I defines the computational cost of IMV.

In **the interpretable results generation phase**, the complexity is $O(S)$, where S is the number of selected features. - Overall, the theoretical time complexity of the OTPat-based XFE model is $O(D \cdot L \cdot C + N \cdot D + R \cdot K \cdot D + L \cdot D + P \cdot K + I + S)$. While this analysis suggests that computational effort increases linearly with these dimensions, the total complexity depends on implementation details and dataset size.

We have used these functions (i) main, (ii) OTPat, (iii) CWINCA, (iv) tkNN, and (v) explainable results generation to develop our proposed model. These functions are stored as .m files and CPU mode was used to execute the OTPat-driven XFE model. The explainable results generation function was configured to ensure accurate results for various datasets.

To evaluate this lightweight model, we used classification accuracy, F1-score, recall, precision, and geometric mean as performance metrics. Figure 3 presents the confusion matrices obtained using our introduced OTPat-based XFE framework.

By utilizing these confusion matrices, the error analyses of these datasets are:

EEG Stress dataset:

- Figure 3a shows 22 (1.23% error rate) stressed segments were wrongly predicted as control.
- 12 control (0.64% error rate) segments were incorrectly predicted as stress.
- There were 34 errors out of 3,667 segments (0.93% error rate).
- One error source may be the subtle overlap in EEG patterns between stressed and non-stressed states. Another error source is explained as follows. This dataset was labeled using participants' declarations.

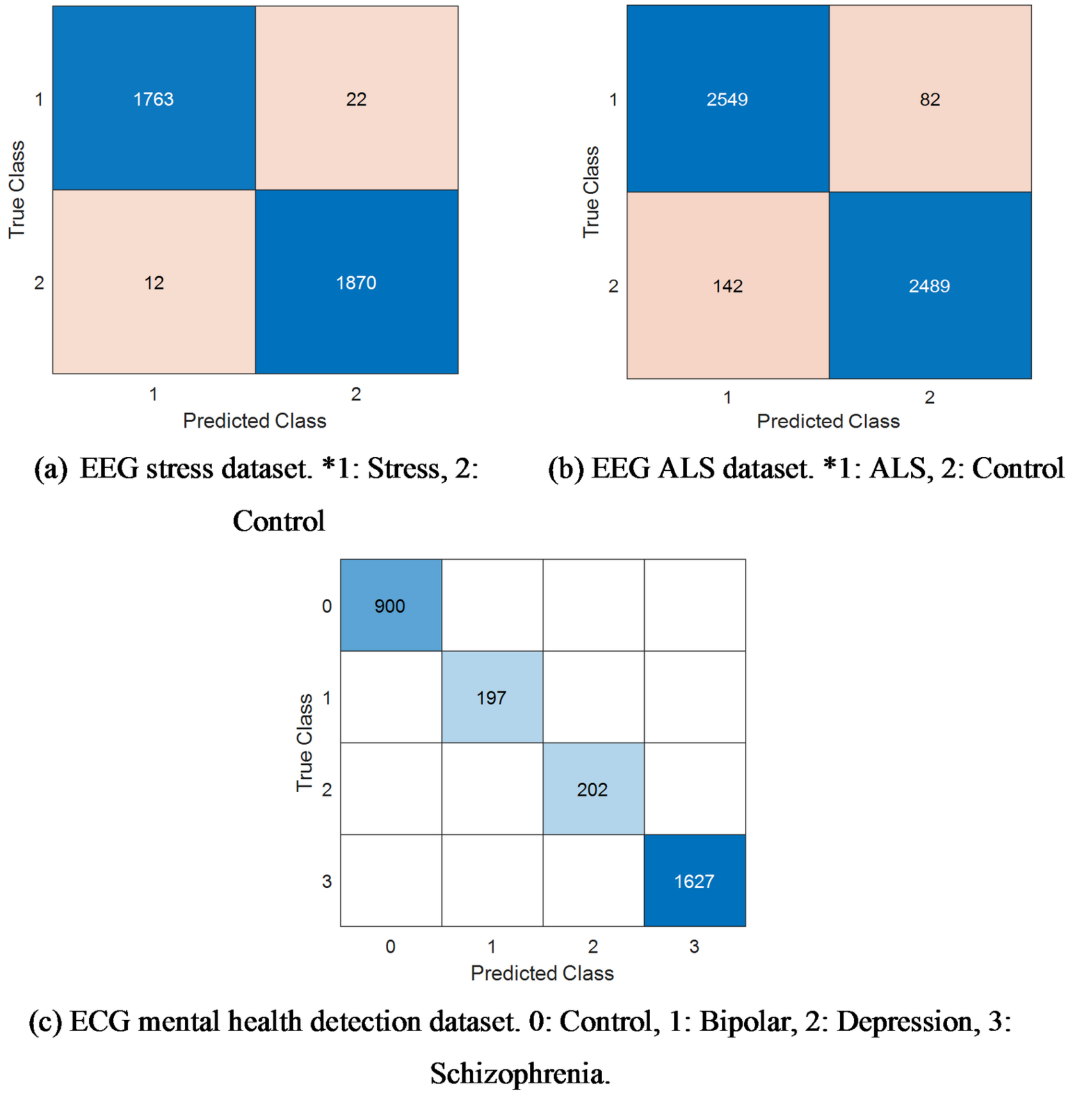

Fig. 3. Confusion matrices obtained using our introduced OTPat-based XFE framework.

- Another factor is the natural variability in participants' emotional responses.

EEG ALS dataset:

- Figure 3b indicates 82 (3.11% error rate) ALS segments were predicted as control.
- 142 (5.40% error rate) control segments were predicted as ALS.
- This results in 224 errors out of 5,262 segments (4.26% error rate).
- Some ALS participants may have mild or unusual EEG patterns that confuse the model.
- Control group signals may sometimes resemble ALS due to occasional anomalies, noise, or the model's inability to discriminate certain specific patterns.

ECG Mental Health:

- Figure 3c shows complete accuracy across all four classes (normal, bipolar, depression, and schizophrenia).
- There were no errors under the tested conditions. Since this dataset contains ECG beats.
- This perfect classification might result from strong class separation in the ECG signals.
- It might also be due to having enough training data for each category.
- Future work should test the model on more varied cardiac patterns to ensure robust generalization.

Table 2 represents the performances (%) obtained using the confusion matrices shown in Fig. 3.

The results illustrate that the introduced OTPat-based XFE framework achieved over 95% classification accuracies, F1-scores, and geometric means across all three datasets used. Furthermore, the introduced OTPat-based XFE framework attained 100% classification performance for the ECG mental health dataset. These results were obtained using 10-fold cross-validation.

Metric	EEG stress	EEG ALS	ECG mental health
Classification accuracy	99.07	95.74	100
Recall	98.77	94.60	100
Precision	99.32	94.72	100
F1-score	99.04	95.79	100
Geometric mean	99.06	95.73	100

Table 2. Results (%) obtained for the proposed model using different datasets.

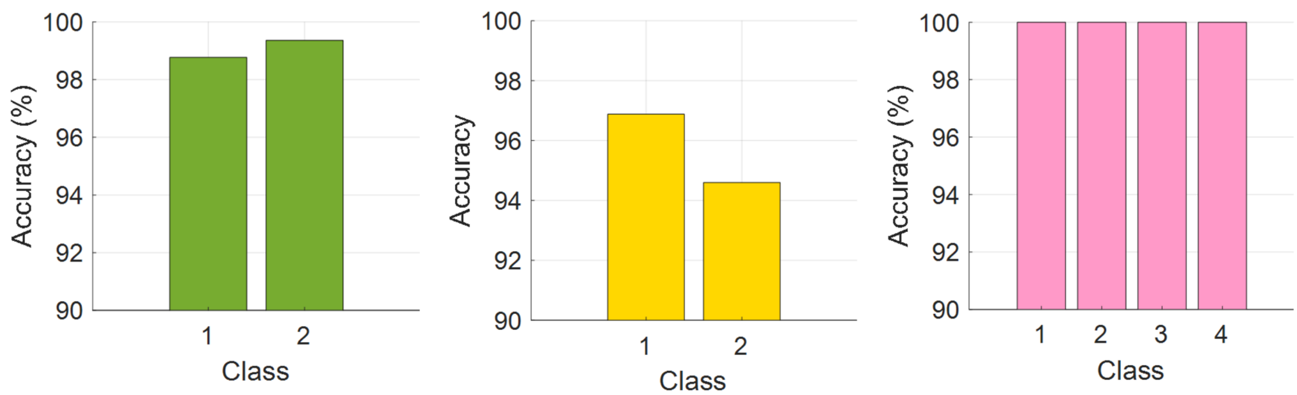

(a) EEG stress dataset. 1: Stress, 2: Control

(b) EEG ALS dataset. 1: ALS, 2: Control

(c) ECG mental health detection dataset. 0: Control, 1: Bipolar, 2: Depression, 3: Schizophrenia.

Fig. 4. Class-wise accuracies obtained using the presented OTPat-driven XFE model.

Also, the class-wise accuracies of these datasets are shown in Fig. 4.

The second set of results pertains to XAI outcomes. To generate these results, DLob was used for XAI analysis of the EEG datasets, and Cardioish was used to obtain interpretable results from the ECG dataset. The obtained interpretable results are illustrated in Fig. 5.

As shown in Fig. 5, interpretable results were extracted using DLob and Cardioish. According to these results:

Frontal activations are the most frequent in earthquake-based stress detection.

For ALS detection, frontal and parietal activations are more prominent than other regions.

ECG-based mental health detection is the most complex process, as the distribution of the Cardioish symbols resembles a uniform distribution. In this classification process, the most frequently used Cardioish symbol is Ld2 (Lead 2).

Table 3 shows the entropies extracted from the symbolic language strings.

Table 3 demonstrates that the EEG stress string is the most predictable, with a complexity ratio of 83.91%. The most complex extracted string belongs to the ECG mental health detection dataset, with a complexity ratio of 99.49%. In the EEG datasets, ALS detection is more complicated than stress detection, as ALS is a complex disorder.

Discussions

We evaluated our presented a new OTPat-driven XFE model using time complexity, classification performance, and explainable results.

Our proposed XFE model has linear time complexity and is more efficient than deep learning models, which typically have exponential time complexities.

We used two EEG datasets and one ECG dataset to demonstrate the general classification ability of the proposed OTPat-driven model. Our model achieved classification accuracies of 99.07%, 95.74%, and 100% on the EEG stress, EEG ALS, and ECG mental health datasets, respectively. These results demonstrate the effectiveness of the proposed model in achieving high classification performance. Hence, this proposed model is an alternative to deep learning models and maintains linear time complexity.

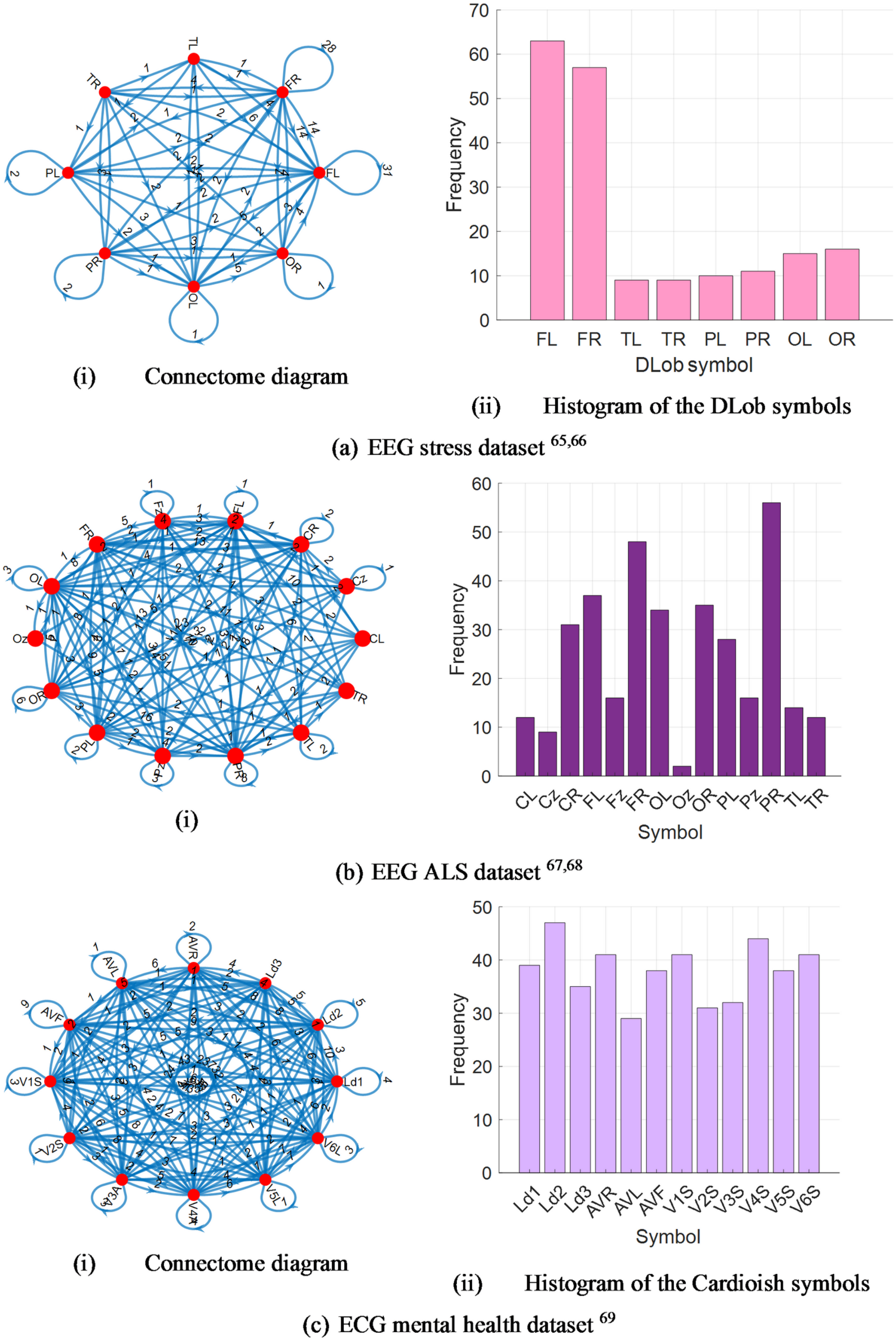

Fig. 5. Computed explainable results.

To validate the introduced OTPat-centric XFE framework's high classification performance, we applied statistical tests to the datasets. For the EEG Stress dataset, the z-value is 11.31 and the p-value is about 10^{-28}. For the EEG ALS dataset, the z-value is 2.47 and the p-value is 0.013. For the ECG Mental Health dataset, the z-value is 13.44 and the p-value is about 10^{-40}.

A connectome diagram was generated for each dataset. Additionally, strings were created for these datasets, and the complexity of the generated strings was analyzed using Shannon entropy.

Table 4 shows the comparison of our results with the state-of-the-art techniques.

Dataset	Entropy	Number of symbols	Maximum entropy	Ratio
EEG stress dataset	2.5173	8	3	0.8391
EEG ALS dataset	3.5238	14	3.8074	0.9255
ECG mental health detection dataset	3.5667	12	3.5850	0.9949

Table 3. Summary of various entropies computed for different datasets.

Model	Year	Method	Accuracy (%)	XAI
EEG Stress dataset				
Cambay et al. [65]	2024	QuadTPat + CWNCA + tkNN	10-fold CV: 92.94 LOSO CV: 73.63	DLob-based XAI generation
Bektas et al. [66]	2024	ChMinMaxPat + CWNCA + tkNN + IMV	10-fold CV: 92.86 LOSO CV: 73.30	DLob-based XAI generation
Our model		OTPat + CWINCA + tkNN	10-fold CV: 99.07 LOSO CV: 76.87	DLob-based XAI generation
EEG ALS dataset				
Samanta et al. [72]	2023	3D CNN	20:3:3: 80.20	-
Our model		OTPat + CWINCA + tkNN	10-fold CV: 95.74	DLob-based XAI generation
ECG Mental Health Dataset				
Tuncer et al. [17]	2024	Transition table feature extraction + INCA feature selector + kNN classifier	10-fold CV: 99.62	Cardioish-based XAI generation
Tasci et al. [69]	2024	MDWT and ternary pattern feature extraction + IChi2 feature selection + ANN classifier + IMV	10-fold CV: 96.25	-
Our model		OTPat + CWINCA + tkNN	10-fold CV: 100	Cardioish-based XAI generation

Table 4. Comparative results. **ChMinMaxPat: Channel-based minimum and maximum pattern, CWNCA: Cumulative Weighted Minimum and Maximum Pattern, IMV: Iterative Majority Voting, QuadTPat: Quadruple Transition Pattern, INCA: Iterative Neighborhood Component Analysis, MDWT: Multilevel Discrete Wavelet Transform, IChi2: Iterative Chi2 feature selector, ANN: Artificial Neural Network.

Table 4 demonstrates high classification performance and provides explainable results using our proposed model.

In the LOSO CV strategy, each participant's data is used only once as the test set. It introduces more within-subject variability than a k-fold CV with random splits. Various participants have different physiological patterns, signal amplitudes, and noise features. These variations make it hard for the model to generalize while training subjects using the unseen subject. As a result, classification accuracy may decrease because the model is exposed to fewer unique subject-specific features.

But, during the 10-fold CV, the same participant's EEG/ECG signals can be used in both training and testing sets. This overlap improves performance of the model.

We used DLob and Cardioish symbolic languages to obtain explainable results. The explanations of Cardioish and DLob substrings are displayed below.

The DLob string for stress detection is discussed below:

FLFLFLFLFLFRFLFLOLOR: This substring begins with FL dominance, reflecting logical reasoning and planning activities. The transition to FR indicates involvement in emotional regulation and creative thinking. OL and OR suggest visual processing, which is likely related to evaluating external stimuli during stress. This pattern represents heightened cognitive engagement and sensory input evaluation.

FRFRFRFRORPRFRFRTRPR: The repeated FR indicates a focus on emotional responses and creative problem-solving. OR and PR signify sensory and visual processing, while TR reflects auditory and emotional input. This substring likely corresponds to stress-induced emotional responses and situational assessment.

FLFLFLFLTLFLPORFLFL: The presence of FL and TL highlights logical thinking and memory retrieval, possibly tied to analyzing the source of stress. PR and OR indicate sensory integration and visual processing. This sequence suggests the brain's effort to process and evaluate the stressor logically.

FRFRFLFLFRFRFRFLFRTRPL: The dominant usage of the FL and FR highlights logical reasoning. TR and PL add auditory processing.

TLFRFRFLORFRFROROLFR: This pattern defines attempts to link sensory input with emotional evaluation under stress.

FRTLPLTLFLFLFLFRFRPL: The presence of TL and PL indicates the integration of auditory and sensory input, while FL and FR suggest logical-emotional coordination. This pattern defines an active mental processing with stress.

ORFLFLOLFLTRORFRFRFLFL: During the data collection phase, videos were shown to participants. This pattern explains the interpretation of visual inputs.

TLFLFLFLFLTLOLPLFRFRFR: This pattern corresponds to efforts to maintain control and process external stress-inducing stimuli.

These findings highlight strong activations in frontal (FL, FR), parietal (PL, PR), temporal (TL, TR), and occipital (OL, OR) regions. The frequent involvement of FR and FL underscores the brain's efforts to balance emotional responses with logical decision-making under stress. Sensory integration using parietal and occipital regions indicates active environmental monitoring.

For EEG ALS detection, the generated sample substrings are explained below:

TLFzFRTROLPRORFRFzFLFLPL: This substring/pattern begins with TL and Fz, indicating memory processing, attention control, and higher cognitive functions. FR reflects emotional involvement, while TR suggests auditory and emotional cues. PL showcases sensory input integration, particularly tactile or spatial awareness. In ALS, this combination may correspond to the brain's effort to compensate for declining motor functions with heightened cognitive and sensory awareness.

OLFRPRORFRPRFLFRCRPRFRTRCR: The presence of OL and FR highlights visual input processing and emotional engagement, possibly due to the data collection environment. PR indicates sensory integration. Repeated transitions between CR and FR suggest disrupted motor actions and emotional regulation, often affected in ALS due to corticospinal tract degeneration.

PRCzFRPzCRPRPRORFLPLPLFRTRFzPL: These activities may represent the brain's struggle to coordinate declining motor functions while engaging cognitive regions for compensation.

OLFRPRFzCRPRFLTLORFRTRPRORCz: This pattern suggests disrupted motor planning and coordination, a hallmark of ALS progression.

FLTLTRFLOLPRPRFRCRFzPRPRPRFRPL: In ALS, this pattern defines the brain's effort to manage motor impairments while maintaining emotional and cognitive processing.

These patterns highlight the neurological adaptations and impairments associated with ALS.

For ECG mental health classification, the generated Cardioish substrings are as follows:

V2SAVFLd2AVLAVLAVRLd3Ld2AVFLd1: This sequence is associated with normal cardiac activity. The recurring and balanced transitions between AVF and AVL indicate regular electrical activity.

Ld3AVRAVRAVFV2SLd3AVLAVRLd1V5SV2S: This segment exhibits repeated transitions between AVR and AVF, along with mismatches between septal and lateral leads, suggesting bipolar disorder.

AVFV2SAVFV2SV2SAVLLd3V6SV5SV2SAVFAVLV1SLd2AVR: This sequence shows a suppressed and repetitive pattern. The loop involving AVL, V2S, and AVF aligns with depression, characterized by lower variability and steadiness rather than irregularity.

V3SV4SV3SV1SLd3AVFV3SV1SV6SLd1V1SAVLAVLLd2V2SAVFV1SAVLLd2: High repetition, chaotic transitions, and mismatched electrical signals point toward schizophrenia. The frequent transitions between various leads and the elevated entropy level are characteristic of this class.

V6SV5SV6SV3SAVFAVLV3SV1SAVFAVLV2SAVLV1SAVRLd3Ld2V2SV2SV3SV5SV6S: Repeated and orderly transitions are observed. The overall structure appears balanced, reflecting normal cardiac activity.

These Cardioish substrings highlight how cardiac patterns mirror mental states, underscoring the potential for non-invasive mental health assessment through advanced cardiac signal analysis.

Test of the additional dataset

The EEG signal dataset used in this study has two classes. To demonstrate the classification ability of the proposed OTPat-driven XFE model on a diverse dataset, we used an EEG artifact classification dataset[16], which contains eight classes. These classes include one control class and seven artifact classes. The proposed OTPat-driven XFE model was applied to this EEG artifact dataset, and the computed confusion matrix and the explainable results, are presented in Fig. 6.

The findings from these results are as follows:

- For artifact classification, the dominant symbols are FL and FR.
- The information entropy of the generated DLob string for artifact detection is calculated as 2.7394. Here, 8 DLob symbols have been used. Consequently, the maximum entropy is computed as 3 (=$\log_2 8$). Therefore, the complexity ratio of the generated DLob string is 91.31%.
- The proposed OTPat-driven XFE model achieved a classification accuracy of 86.07% and a geometric mean of 75.26%.

To showcase the high classification performance of the OTPat-based model, comparative results are provided in Table 5.

Table 5 shows that the recommended OTPat-driven XFE model achieved approximately 8.5% higher classification accuracy and a 15% higher geometric mean than the TTPat-based XFE model. These results and comparative results have highlighted the high classification ability of the introduced OTPat feature extractor.

Highlights

The salient features of the proposed OTPat-driven XFE model are given below.

- Presents a new model for classifying biomedical signals (EEG and ECG) with high performance.
- The proposed XFE model employed symbolic languages to obtain interpretable results.
- Innovative part of the model is the OTPat feature extractor, which captures important features from both signal channels and the signals themselves using ordering coding and transition table extraction methods.
- The model selects the best features using the CWINCA feature selector.
- The tkNN, a self-organized and improved version of the kNN classifier, is used for classification.
- The model includes XAI techniques using two symbolic languages: DLob for EEG and Cardioish for ECG.
- These symbolic languages help generate interpretable results, called connectome diagrams.

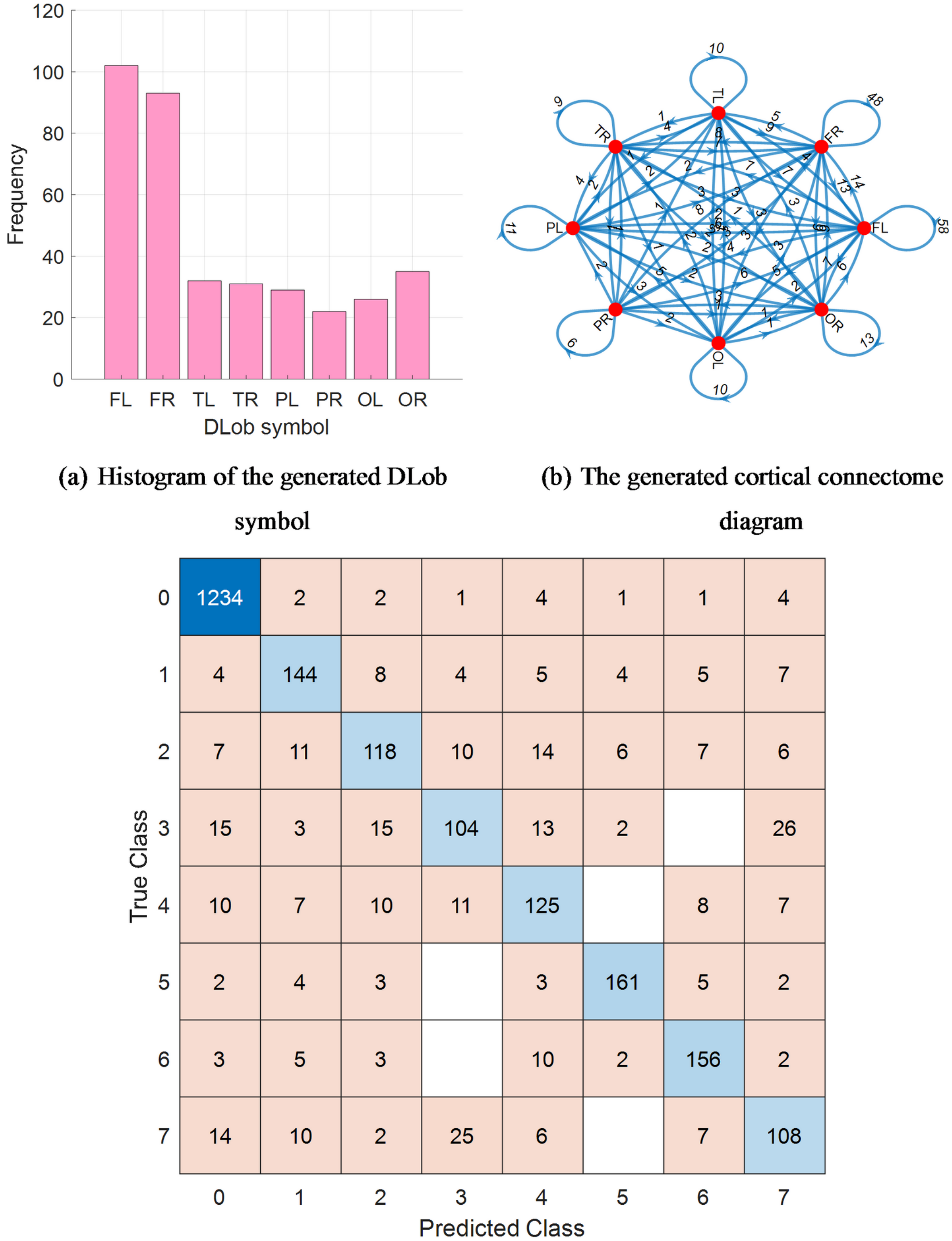

(a) Histogram of the generated DLob symbol

(b) The generated cortical connectome diagram

(c) Confusion matrix.

** 0: No Artifact, 1: Limb Tremor, 2: Noise, 3: Body Movement, 4: Eye Blinking, 5: Swallowing, 6: Vertical Eye Movement, 7: Speaking

Fig. 6. Results of the OTPat-driven XFE for artifact classification dataset.

- Proposed OTPat-based model achieved over 95% accuracy on the three datasets.
- Introduced OTPat-driven XFE model is efficient because it has linear time complexity, making it faster than many deep learning models.
- Addresses gaps in the current research by being multimodal (working with different types of signals) and provides interpretable results.
- OTPat-driven XFE model is an alternative to deep learning models, requiring less computational power. Moreover, this model achieved high classification accuracy due to its self-organized nature.

Model	Year	Method	Results (%)	XAI
Tuncer et al. [16]	2024	TTPat + CWNCA + tkNN	Accuracy: 77.58 Geometric mean: 60.09	DLob-based XAI generation
Our model		OTPat + CWINCA + tkNN	Accuracy: 86.07 Geometric mean: 75.26	DLob-based XAI generation

Table 5. Comparative results for EEG artifact detection.

- The presented model attained satisfactory classification performance in comparison to other methods.
- The explainable results provide medical insights, aiding in a better understanding of the signals.

Findings of the explainable results are discussed below:

- The interpretable results demonstrate the effectiveness of the OTPat-driven XFE model in capturing meaningful patterns from biomedical signals.
- Symbolic representation (using DLob and Cardioish) of complex data facilitates easier interpretation and supports medical decision-making.
- The introduced OTPat-driven XFE model presents a promising approach for the noninvasive detection and analysis of neurological and mental health conditions.
- The patterns show strong activations across multiple brain regions, indicating that stress induces a comprehensive neurological response involving cognitive, emotional, and sensory processing.
- Frequent transitions between frontal regions suggest efforts to manage stress through reasoning and emotional regulation.
- ALS affects multiple neural pathways, resulting in complex activation patterns.
- The symbolic sequences reveal neurological adaptations, with increased engagement of cognitive and sensory regions to mitigate motor impairments in ALS.
- Two custom generative pretrained transformers (GPTs) have been developed for DLob (https://chatgpt.com/g/g-E3Gvijurs-lobish-eeg-interpreter) and Cardioish (https://chatgpt.com/g/g-A07G0SK6l-cardioish-sembolik-kardiyoloji-dili).
- Cardiac activity varies significantly across different mental health conditions.
- The complex and unique patterns in Cardioish sequences highlight the potential for ECG-based non-invasive mental health assessments.

Limitations

- Obtained the lower classification accuracy of 76.87% using LOSO CV.
- Generated XAI results using DLob and Cardioish symbolic languages. However, it is challenging to translate these results.

Future directions

- New generation models can be developed to improve the classification ability of the presented OTPat-driven XFE model using LOSO CV. One solution is to collect more data from a broader range of participants. A larger and more diverse dataset can reduce overfitting to a small group. Data augmentation techniques can help mimic differences between subjects. Techniques such as synthetic signal generation, random clipping, and adding realistic noise are helpful. Domain adaptation methods can align feature distributions from different subjects. Subject-specific fine-tuning is another option. In this method, a small portion of each test subject's data is used to adapt the model. This helps the model account for individual physiological differences while keeping a general framework. Finally, regularization strategies like dropout or L2 penalty can improve model robustness and reduce overfitting to any subject[73].
- A new graphical user interface (GUI) can be created to simplify translating generated Cardioish and DLob sentences. This approach will make it easier to interpret ECG and EEG data. The GUI can also support the development of educational applications.
- We plan to create a comprehensive DLob and Cardioish dictionaries to detect conditions, with unique patterns showcased in these dictionaries.
- New-generation OTPat-driven deep learning models can be developed. OTPat and similar methods can be utilized as operators in deep learning architectures instead of the convolution operator.
- Personalized healthcare applications can be developed using our model. These applications will provide tailored diagnostic and monitoring solutions.

Potential implications

- The OTPat-driven XFE framework developed using EEG/ECG signals can be integrated into clinical workstations.
- Our proposed approach can help healthcare providers detect stress or neurological conditions faster and accurately.
- The explainable results of the model can assist the clinicians in understanding complex EEG and ECG patterns.

- Symbolic languages (DLob and Cardioish) can provide superior diagnostic confidence by providing interpretable visualizations. These visual interpretable outputs (connectome diagrams) can help make accurate diagnoses and in early interventions and treatments.

- This system can assist in telemedicine services in providing faster and accurate remote patient monitoring.
- The developed OTPat-based model can be employed in hospitals and research centers to improve the analysis of stress-related EEG data. Moreover, this model can be utilized to extract more meaningful features from ECG signals.
- The introduced model is suitable for real-time applications as it has the linear time complexity.
- This model can be used in other personalized healthcare platforms to adaptively learn and increase individual patient outcomes.

Conclusions

A novel OTPat-driven XFE model has been proposed for biomedical signal classification and the generation of explainable results. The presented OTPat-driven XFE model achieved more than 95% classification accuracy across all three datasets. We achieved an accuracy of 99.07%, 95.74%, and 100% for the EEG stress dataset, EEG ALS dataset, and ECG mental health datasets, respectively, with a 10-fold cross-validation strategy. Furthermore, the OTPat-driven XFE model achieved 86.07% accuracy on the EEG artifact detection dataset, which consists of 8 classes.

The interpretable results generated using the DLob and Cardioish symbolic languages provided insights into neurological and cardiac activity patterns. For example, frequent transitions were observed in the frontal regions during stress detection, indicating efforts to manage stress through reasoning and emotional regulation. Symbolic sequences for ALS detection demonstrated neurological adaptations, including increased activation of cognitive and sensory regions to compensate for motor impairments. In mental health classification, Cardioish sequences demonstrated changes in cardiac activity across different conditions, including bipolar disorder, depression, and schizophrenia.

The model's linear time complexity ensures computational efficiency compared to deep learning approaches. Additionally, the combined use of DLob and Cardioish symbolic languages highlights their utility as XAI methods, demonstrating how such symbolic approaches contribute to explainable artificial intelligence.

The results indicate that the OTPat-driven XFE model can be a practical tool for the non-invasive analysis of neurological and mental health conditions. Its high classification accuracy, combined with interpretable outputs, positions the model as a reliable tool for medical implementations.

Data availability

No new datasets were generated during the current study. Consequently, the authors do not hold the rights to share the datasets used. For data access inquiries, contact the corresponding author.

Received: 13 January 2025; Accepted: 24 April 2025
Published online: 01 May 2025

References

1. Popov, A. & Ivanko, K. *In Advances in Artificial Intelligence*. 1–57 (Elsevier, 2024).
2. Rangayyan, R. M. & Krishnan, S. *Biomedical Signal Analysis*. (Wiley, 2024).
3. Wu, H. Multiscale entropy with electrocardiograph, electromyography, electroencephalography, and photoplethysmography signals in healthcare: A twelve-year systematic review. *Biomed. Signal Process. Control*. **93**, 106124 (2024).
4. Kumar, A., Koch, N., Imran, S. & Yadav, J. in *Evolution of Machine Learning and Internet of Things Applications in Biomedical Engineering* 145–168. (CRC Press, 2024).
5. Ardeti, V. A., Kolluru, V. R., Varghese, G. T. & Patjoshi, R. K. An overview on state-of-the-art electrocardiogram signal processing methods: traditional to AI-based approaches. *Expert Syst. Appl.* **217**, 119561 (2023).
6. Chaddad, A., Wu, Y., Kateb, R. & Bouridane, A. Electroencephalography signal processing: A comprehensive review and analysis of methods and techniques. *Sensors* **23**, 6434 (2023).
7. Sharma, R. & Meena, H. K. Emerging trends in EEG signal processing: A systematic review. *SN Comput. Sci.* **5**, 1–14 (2024).
8. Duan, J., Xiong, J., Li, Y. & Ding, W. Deep learning based multimodal biomedical data fusion: an overview and comparative review. *Inform. Fusion*, 102536 (2024).
9. Ranjan, R., Sahana, B. C. & Bhandari, A. K. Deep learning models for diagnosis of schizophrenia using EEG signals: emerging trends, challenges, and prospects. *Arch. Comput. Methods Eng.* **31**, 2345–2384 (2024).
10. Basri, S. M. M., Al-Nashash, H. & Mir, H. Inverse problem for M/EEG source localization: A review. *IEEE Sens. J.* (2024).
11. AlSaad, R. et al. Multimodal large Language models in health care: applications, challenges, and future outlook. *J. Med. Internet. Res.* **26**, e59505 (2024).
12. Vashishth, T. K., Sharma, V. & Ahamad, S. Exploring machine learning models for biomedical signal processing: a comprehensive review. *Mach. Learn. Models Architectures Biomedical Signal. Process.*, 69–96 (2025).
13. Minissi, M. E. et al. Biosignal comparison for autism assessment using machine learning models and virtual reality. *Comput. Biol. Med.* **171**, 108194 (2024).
14. Cambay, V. Y., Baig, H., Aydemir, A., Tuncer, E., Dogan, S. & T. & Minimum and maximum Pattern-Based Self-Organized feature engineering: fibromyalgia detection using electrocardiogram signals. *Diagnostics* **14**, 2708 (2024).
15. Tuncer, T. et al. Lobish: symbolic Language for interpreting electroencephalogram signals in Language detection using Channel-Based transformation and pattern. *Diagnostics* **14**, 1987 (2024).
16. Tuncer, T. et al. Directed Lobish-based explainable feature engineering model with TTPat and CWINCA for EEG artifact classification. *Knowl. Based Syst.* **305**, 112555 (2024).
17. Tuncer, T. et al. Cardioish: Lead-Based feature extraction for ECG signals. *Diagnostics* **14**, 2712 (2024).
18. Gupta, V., Kanungo, A., Kumar, P., Kumar, N. & Choubey, C. A design of bat-based optimized deep learning model for EEG signal analysis. *Multimedia Tools Appl.* **82**, 45367–45387 (2023).

19. Gupta, V. et al. A firefly based deep belief signal specification based novel hybrid technique for EEG signal analysis. *IETE J. Res.* **70**, 5263–5269 (2024).
20. Malan, N. & Sharma, S. *Motor Imagery EEG spectral-spatial Feature Optimization Using dual-tree Complex Wavelet and Neighbourhood Component Analysis*. 43198–209 (IRBM, 2022).
21. Ma, P. et al. Effect of local network characteristics on the performance of the SSVEP brain-computer interface. *IRBM* **44**, 100781 (2023).
22. Akbari, H. et al. Recognizing seizure using poincaré plot of EEG signals and graphical features in DWT domain. *Bratislava Med. Journal/Bratislavske Lekarske Listy*. **124**, 12–24 (2023).
23. Akbari, H. et al. Depression detection based on geometrical features extracted from SODP shape of EEG signals and binary PSO. *Traitement Du Signal.* **38**, 13–26 (2021).
24. Sadiq, M. T. et al. Exploiting pretrained CNN models for the development of an EEG-based robust BCI framework. *Comput. Biol. Med.* **143**, 105242 (2022).
25. Sadiq, M. T., Yu, X., Yuan, Z. & Aziz, M. Z. Motor imagery BCI classification based on novel two-dimensional modelling in empirical wavelet transform. *Electron. Lett.* **56**, 1367–1369 (2020).
26. Sadiq, M. T., Akbari, H., Siuly, S., Li, Y. & Wen, P. Alcoholic EEG signals recognition based on phase space dynamic and geometrical features. *Chaos Solitons Fractals*. **158**, 112036 (2022).
27. Kundu, S. & Ari, S. Brain-computer interface speller system for alternative communication: a review. *IRBM* **43**, 317–324 (2022).
28. Sadiq, M. T. et al. Toward the development of versatile brain–computer interfaces. *IEEE Trans. Artif. Intell.* **2**, 314–328 (2021).
29. Yu, X., Aziz, M. Z., Sadiq, M. T., Fan, Z. & Xiao, G. A new framework for automatic detection of motor and mental imagery EEG signals for robust BCI systems. *IEEE Trans. Instrum. Meas.* **70**, 1–12 (2021).
30. Sadiq, M. T. et al. Motor imagery BCI classification based on multivariate variational mode decomposition. *IEEE Trans. Emerg. Top. Comput. Intell.* **6**, 1177–1189 (2022).
31. Sadiq, M. T. et al. Motor imagery EEG signals decoding by multivariate empirical wavelet transform-based framework for robust brain–computer interfaces. *IEEE Access.* **7**, 171431–171451 (2019).
32. Bashir, N. et al. A machine learning framework for major depressive disorder (MDD) detection using non-invasive EEG signals. *Wireless Pers. Commun.* 1–23 (2023).
33. Yadav, S. K. et al. Comparative analysis of signal processing techniques for mental state recognition in Brain-Computer interfaces (BCI). *Wireless Pers. Commun.* **131**, 1569–1592 (2023).
34. Polat, K. & Nour, M. Epileptic seizure detection based on new hybrid models with electroencephalogram signals. *Irbm* **41**, 331–353 (2020).
35. Narin, A. Detection of focal and non-focal epileptic seizure using continuous wavelet transform-based scalogram images and pre-trained deep neural networks. *Irbm* **43**, 22–31 (2022).
36. Faust, O., Acharya, R., Allen, A. R. & Lin, C. Analysis of EEG signals during epileptic and alcoholic States using AR modeling techniques. *Irbm* **29**, 44–52 (2008).
37. Gupta, V., Kanungo, A., Saxena, N. K., Kumar, P. & Kumar, P. An adaptive optimized schizophrenia electroencephalogram disease prediction framework. *Wireless Pers. Commun.* **130**, 1191–1213 (2023).
38. Chandran, K. S. & Perumalsamy, M. EEG based strategies for human gustation classification using Spartan—6 FPGA. *Wireless Pers. Commun.* **103**, 3041–3053 (2018).
39. Khare, S. & Bajaj, V. Optimized tunable Q wavelet transform based drowsiness detection from electroencephalogram signals. *Irbm* **43**, 13–21 (2022).
40. Ma, X., Rizzoglio, F., Bodkin, K. L. & Miller, L. E. Unsupervised, piecewise linear decoding enables an accurate prediction of muscle activity in a multi-task brain computer interface. *J. Neural Eng.* (2025).
41. Mane, S. A. M., Shinde, A. & StressNet Hybrid model of LSTM and CNN for stress detection from electroencephalogram signal (EEG). *Results Control Optim.* **11**, 100231 (2023).
42. Badr, Y. et al. A review on evaluating mental stress by deep learning using EEG signals. *Neural Comput. Appl.*, 1–26 (2024).
43. Malviya, L. & Mal, S. A novel technique for stress detection from EEG signal using hybrid deep learning model. *Neural Comput. Appl.* **34**, 19819–19830 (2022).
44. Roy, B. et al. Hybrid deep learning approach for stress detection using decomposed Eeg signals. *Diagnostics* **13**, 1936 (2023).
45. Fernandez, J., Martínez, R., Innocenti, B. & López, B. Contribution of EEG Signals for Students' Stress Detection. *IEEE Trans. Affect. Comput.* (2024).
46. Patel, A., Nariani, D. & Rai, A. in *IEEE Applied Sensing Conference (APSCON).* 1–3 (IEEE, 2023).
47. Al-Saggaf, U. M., Naqvi, S. F., Moinuddin, M., Alfakeh, S. A. & Ali, S. S. A. Performance evaluation of EEG based mental stress assessment approaches for wearable devices. *Front. Neurorobotics.* **15**, 819448 (2022).
48. Opałka, S., Stasiak, B., Szajerman, D. & Wojciechowski, A. Multi-channel convolutional neural networks architecture feeding for effective EEG mental tasks classification. *Sensors* **18**, 3451 (2018).
49. Zhang, P., Wang, X., Zhang, W. & Chen, J. Learning spatial–spectral–temporal EEG features with recurrent 3D convolutional neural networks for cross-task mental workload assessment. *IEEE Trans. Neural Syst. Rehabil. Eng.* **27**, 31–42 (2018).
50. He, J., Li, K., Liao, X., Zhang, P. & Jiang, N. Real-time detection of acute cognitive stress using a convolutional neural network from electrocardiographic signal. *IEEE Access.* **7**, 42710–42717 (2019).
51. Bergil, E., Oral, C. & Ergül, E. U. Classification of arithmetic mental task performances using EEG and ECG signals. *J. Supercomputing*. **79**, 15535–15547 (2023).
52. Pirasteh, A., Shamseini Ghiyasvand, M. & Pouladian, M. EEG-based brain-computer interface methods with the aim of rehabilitating advanced stage ALS patients. *Disabil. Rehabilitation: Assist. Technol.*, 1–11 (2024).
53. Ayus, I. & Gupta, D. A novel hybrid ensemble based Alzheimer's identification system using deep learning technique. *Biomed. Signal Process. Control*. **92**, 106079 (2024).
54. Azghadi, M. R. et al. Hardware implementation of deep network accelerators towards healthcare and biomedical applications. *IEEE Trans. Biomed. Circuits Syst.* **14**, 1138–1159 (2020).
55. Krishna, T. B. & Kokil, P. Standard fetal ultrasound plane classification based on stacked ensemble of deep learning models. *Expert Syst. Appl.* **238**, 122153 (2024).
56. Chocron, A. et al. Remote atrial fibrillation burden Estimation using deep recurrent neural network. *IEEE Trans. Biomed. Eng.* **68**, 2447–2455 (2020).
57. Khosravi, M., Parsaei, H., Rezaee, K. & Helfroush, M. S. Fusing convolutional learning and attention-based Bi-LSTM networks for early Alzheimer's diagnosis from EEG signals towards IoMT. *Sci. Rep.* **14**, 26002 (2024).
58. Tuncer, T., Dogan, S., Tasci, I., Tasci, B. & Hajiyeva, R. TATPat based explainable EEG model for neonatal seizure detection. *Sci. Rep.* **14**, 26688 (2024).
59. Ouyang, D. et al. Electrocardiographic deep learning for predicting post-procedural mortality: a model development and validation study. *Lancet Digit. Health*. **6**, e70–e78 (2024).
60. Tuncer, T. et al. TPat: transition pattern feature extraction based Parkinson's disorder detection using FNIRS signals. *Appl. Acoust.* **228**, 110307 (2025).
61. Rana, A. & Kim, K. K. Electrocardiography classification with leaky Integrate-and-Fire neurons in an artificial neural network-Inspired spiking neural network framework. *Sensors* **24**, 3426 (2024).

62. Hooshyar, D. & Yang, Y. Problems with SHAP and LIME in interpretable AI for education: A comparative study of post-hoc explanations and neural-symbolic rule extraction. *IEEE Access.* (2024).
63. Hassija, V. et al. Interpreting black-box models: a review on explainable artificial intelligence. *Cogn. Comput.* **16**, 45–74 (2024).
64. Ortigossa, E. S., Gonçalves, T. & Nonato, L. G. EXplainable artificial intelligence (XAI)–From theory to methods and applications. *IEEE Access.* (2024).
65. Cambay, V. Y. et al. QuadTPat: quadruple transition Pattern-based explainable feature engineering model for stress detection using EEG signals. *Sci. Rep.* **14**, 27320 (2024).
66. Bektas, O. et al. ChMinMaxPat: investigations on violence and stress detection using EEG signals. *Diagnostics* **14**, 2666 (2024).
67. Ngo, T. D. et al. An EEG & eye-tracking dataset of ALS patients & healthy people during eye-tracking-based spelling system usage. *Sci. Data.* **11**, 664 (2024).
68. Le, T. H. *et al. EEGET-ALS Dataset, Figshare*. https://springernature.figshare.com/articles/dataset/EEGET-ALS_Dataset/24485689/1?file=46933189 (2024).
69. Tasci, B., Tasci, G., Dogan, S. & Tuncer, T. A novel ternary pattern-based automatic psychiatric disorders classification using ECG signals. *Cogn. Neurodyn.* **18**, 95–108 (2024).
70. Goldberger, J., Hinton, G. E., Roweis, S. & Salakhutdinov, R. R. Neighbourhood components analysis. *Adv. Neural. Inf. Process. Syst.* **17**, 513–520 (2004).
71. Maillo, J., Ramírez, S., Triguero, I. & Herrera, F. kNN-IS: an iterative Spark-based design of the k-Nearest neighbors classifier for big data. *Knowl. Based Syst.* **117**, 3–15 (2017).
72. Samanta, K. et al. in. *IEEE International Conference on Systems, Man, and Cybernetics (SMC).* 3337–3342 (IEEE, 2023).
73. Asefa, S. H. & Assabie, Y. Transformer-Based Amharic-to-English machine translation with character embedding and combined regularization techniques. *IEEE Access.* (2024).

Author contributions

Author contributions: Mehmet Ali Gelen: Writing– review & editing, Writing– original draft, Visualization, Validation, Resources, Methodology, Investigation, Formal analysis, Data curation, ConceptualizationPrabal Datta Barua: Writing– review & editing, Writing– original draft, Visualization, Validation, Resources, Methodology, Investigation, Formal analysis, Data curation, Conceptualization.Irem Tasci: Writing– review & editing, Writing– original draft, Visualization, Validation, Resources, Methodology, Investigation, Formal analysis, Data curation, Conceptualization.Gulay Tasci: Writing– review & editing, Writing– original draft, Visualization, Validation, Resources, Methodology, Investigation, Formal analysis, Data curation, Conceptualization.Emrah Aydemir: Writing– review & editing, Writing– original draft, Visualization, Validation, Resources, Methodology, Investigation, Formal analysis, Data curation, Conceptualization.Sengul Dogan: Writing– review & editing, Writing– original draft, Visualization, Validation, Software, Resources, Methodology, Investigation, Formal analysis, Data curation, ConceptualizationTurker Tuncer: Writing– review & editing, Writing– original draft, Visualization, Validation, Software, Resources, Methodology, Investigation, Formal analysis, Data curation, Conceptualization. U.R. Acharya: Writing– review & editing, Writing– original draft, Visualization, Validation, Supervision, Resources, Project administration, Methodology, Investigation, Formal analysis, Data curation, Conceptualization.

Declarations

Competing interests

The authors declare no competing interests.

Additional information

Correspondence and requests for materials should be addressed to S.D.